OPERATION and PROPOSALS

1. Outline of the Accelerators

Two electron storage rings, namely the PF ring and the PF-AR, have been stably operated as dedicated light sources at the Photon Factory. The KEK linear accelerator (LINAC) with a maximum electron energy of 8 GeV is employed to inject electron beams into the rings. At the end of FY2016, a full energy injection for the PF-AR became possible by completing a new direct beam transport line from LINAC to PF-AR. Preparations for the simultaneous top-up operation of the PF ring, PF-AR, and SuperKEKB main rings are proceeding.

The machine parameters of the rings and the calculated spectral performances are listed in **Table 1** and **Table 2**, respectively. The spectral distributions of synchrotron radiation (SR) from the bending magnets and the insertion devices are shown in **Fig. 1**.

Table 1: Principal beam parameters of the PF ring and PF-AR.

	PF ring	PF-AR
Energy	2.5 GeV	6.5 GeV
Natural emittance	34.6 nm rad	293 nm rad
Circumference	187 m	377 m
RF frequency	500.1 MHz	508.6 MHz
Bending radius	8.66 m	23.2 m
Energy loss per turn	0.4 MeV	6.66 MeV
Damping time		
Vertical	7.8 ms	2.5 ms
Longitudinal	3.9 ms	1.2 ms
Natural bunch length	10 mm	18.6 mm
Momentum compaction factor	0.00644	0.0129
Natural chromaticity		
Horizontal	–12.9	–14.3
Vertical	–17.3	–13.1
Stored current	450 mA	60 mA
Normal filling	188 bunches (47 × 4)	Single
Beam lifetime	20 h (at 450 mA)	13 h (at 50 mA)
Hybrid filling	Single (50 mA) + 131 bunches (400 mA)	
Beam lifetime	8 h (450 mA)	

Table 2: Calculated spectral performances of the bending source and all the insertion devices at the PF ring (2.5 GeV, 450 mA) and the PF-AR (6.5 GeV, 60 mA). λ_u: period length, *N*: number of periods, *L*: length of undulator or wiggler, $G_y(G_x)$: minimum vertical (horizontal) gap height, $B_y(B_x)$: maximum vertical (horizontal) magnetic field, type of magnet, H: hybrid configuration, S.C.: super-conducting magnet, σ_x, σ_y: horizontal or vertical beam size, $\sigma_{x'}$, $\sigma_{y'}$: horizontal or vertical beam divergence, $K_y(K_x)$: vertical (horizontal) deflection parameter, *D*: photon flux density (photons/sec/mrad^2/0.1%b.w.), *B*: brilliance (photons/sec/mm^2/mrad^2/0.1%b.w.), P_T:total radiated power. Different operating modes of undulator and wiggler are denoted by -U and -W, respectively.

Name	E/I	λ_u	N	L	$G_y(G_x)$	$B_y(B_x)$	Type of magnet	σ_x	σ_y	$\sigma_{x'}$	$\sigma_{y'}$	$K_y(K_x)$	$\varepsilon_1/\varepsilon_c$	D	B	P_T
	GeV/mA	cm		m	cm	T		mm	mm	mrad	mrad		keV			kW
PF	**2.5/450**															
Bend								0.41	0.059	0.178	0.012		4	5.38E+13	3.48E+14	
SGU#01		1.2	39	0.5	0.4	0.7	P(NdFeB)	0.6	0.012	0.088	0.029	0.78		4.56E+16	9.90E+17	0.4
U#02-1		6	60	3.6	2.8	0.4	H(NdFeB)	0.65	0.042	0.054	0.008	2.3		2.73E+17	1.55E+18	1.07
U#02-2		16	17	2.72	2.6	0.33(0.33)	P(NdFeB)	0.65	0.042	0.054	0.008	4.93(4.93)		9.53E+15	4.58E+16	0.53
SGU#03		1.8	26	0.5	0.4	1	P(NdFeB)	0.6	0.012	0.088	0.029	1.68		2.50E+16	5.44E+17	0.82
MPW#05-W		12	21	2.5	2.64	1.4	H(NdFeB)	0.71	0.045	0.078	0.009	16	5.9	2.22E+15	1.10E+16	8.83
U#13		7.6	47	3.6	2.3	0.74(0.51)	P(NdFeB)	0.74	0.02	0.094	0.019	5.28(3.65)		4.46E+16	3.10E+17	3.53
VW#14					5	5	S.C.	0.53	0.045	0.128	0.008		20.8	5.42E+13	3.59E+14	
SGU#15		1.76	27	0.5	0.4	0.97	P(NdFeB)	0.6	0.012	0.088	0.029	1.37		4.38E+15	9.44E+16	0.75
U#16-1 & 16-2		5.6	44	2.5	2.1	0.6(0.38)	P(NdFeB)	0.654	0.042	0.055	0.008	3(2)		1.03E+18	1.82E+17	0.88
SGU#17		1.6	29	0.5	0.4	0.92	P(NdFeB)	0.6	0.012	0.088	0.029	1.37		7.88E+15	1.71E+17	0.69
Revolver#19-B		7.2	32	3.6	2.8	0.4	H(NdFeB)	0.7	0.045	0.078	0.009	2.7		7.17E+16	3.52E+17	0.63
U#28		16	22	3.52	2.7	0.33(0.33)	P(NdFeB)	0.53	0.045	0.127	0.008	4.93(4.93)		1.39E+16	6.59E+16	1.36
PF-AR	**6.5/60**															
Bend								1	0.2	0.593	0.036		26	3.90E+13	3.11E+13	
EMPW#NE01-W		16	21	3.36	3(11)	1(0.2)	P(NdFeB)	1.07	1.07	0.268	0.032	15(3)	28(90%)	1.84E+15	2.54E+15	5.52
U#NE03		4	90	3.6	1	0.8	P(NdFeB)	1.57	0.17	0.312	0.029	3		1.29E+16	7.66E+15	3.708
U#NW02		4	90	3.6	1	0.8	P(NdFeB)	1.57	0.17	0.312	0.029	3		1.29E+16	7.66E+15	3.708
U#NW12		4	95	3.8	1	0.8	P(NdFeB)	1.57	0.17	0.312	0.029	3		1.29E+16	7.66E+15	3.912
U#NW14-36		3.6	79	2.8	1	0.8	P(NdFeB)	1.35	0.14	0.338	0.036	2.8		7.69E+15	6.49E+15	3.12
U#NW14-20		2	75	1.5	0.8	0.63	P(NdFeB)	0.75	0.07	0.383	0.038	1.17		7.69E+15	6.49E+15	0.936

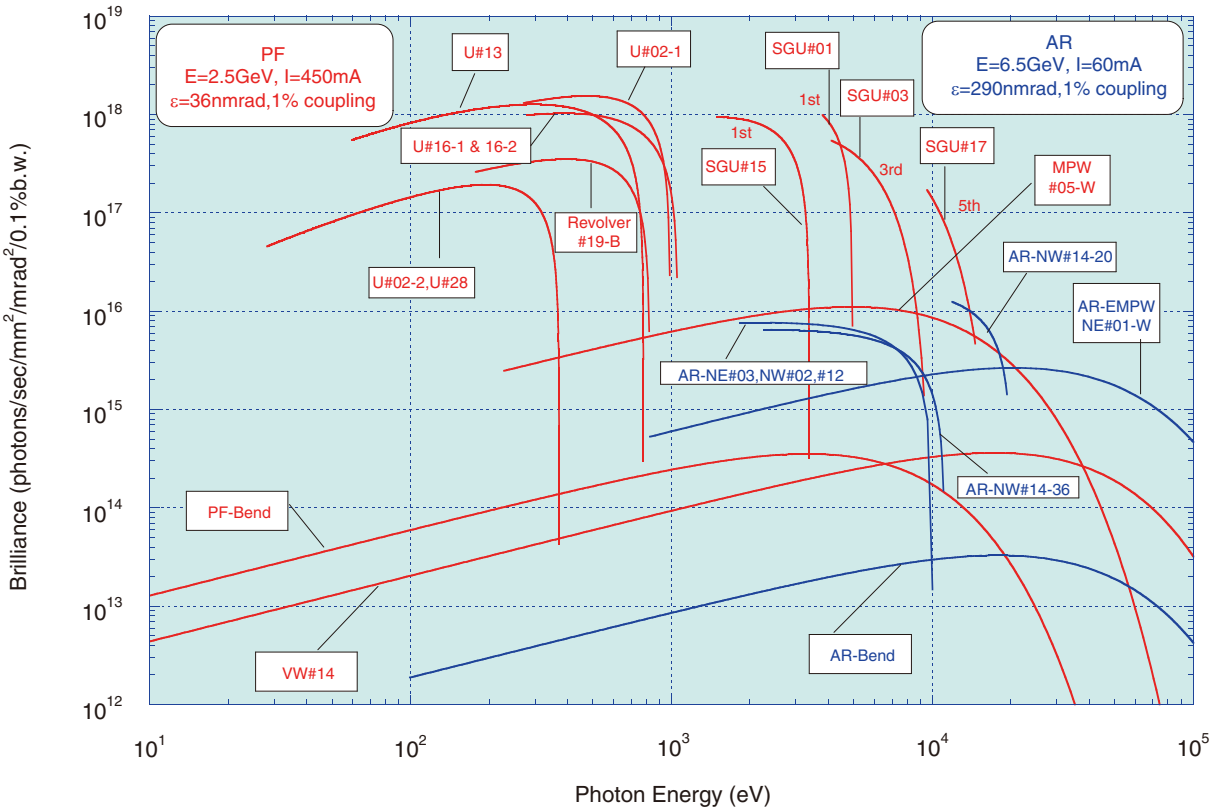

Figure 1: Synchrotron radiation spectra available at the PF ring (2.5 GeV) and the PF-AR (6.5 GeV). Brilliance of the radiation vs. photon energy is denoted by red curves for the insertion devices SGU#01, U#02-1 & 02-2, SGU#03, MPW#05, U#13, VW#14, SGU#15, U#16-1 & 16-2, SGU#17, Revolver#19-B and U#28, and the bending magnets (PF-Bend) at the PF ring. Blue curves denote those for the insertion devices EMPW#NE01, U#NE03, U#NW02, U#NW12, U#NW14-36 and U#NW14-20, and the bending magnets (AR-Bend) at the PF-AR. The name of each source is listed in Table 2. The spectral curve of each undulator (or undulator mode of multipole wiggler) is the locus of the peak of the first harmonic within the allowance range of parameter K. For SGU#01 and SGU#15, the first harmonic regions are shown. For SGU#03, the third harmonic region is shown. For SGU#17, the fifth harmonic region is shown. The spectrum of Revolver#19 for surface B is shown.

2. Operation Summary

The operation schedule of the PF ring and PF-AR in FY2017 is shown in **Fig. 2**. The statistics of the accelerator's operation for the past decade are shown in **Fig. 3**. The scheduled user times in the PF ring were almost the same as those in FY2016. In the PF-AR, the times increased by about 1000 hours following completion of the new direct beam transport line for the PF-AR.

In the PF ring, more detailed operation statistics and the number of failures from FY2007 to FY2017 are listed in **Table 3** and **Table 4**, and a pie chart of the down time in FY2017 is shown in **Fig. 4**. The mean time between failures (MTBF) was over 200 hours, and the failure rate was 0.6%, which remained a low value as usual.

In FY2017, two vacuum troubles of aged accelerator components occurred though they did not affect the failure time for the PF ring. One was corrosion of the aluminum vacuum chamber of the superconducting wiggler. A slow leakage was observed repeatedly after the earthquake of 2011 both in the ring vacuum and the thermal isolation vacuum chambers. Though the operation had continued with a temporary sealing for years, it was stopped in December 2016 to prevent any risk of secondary damage. The recovery work was conducted during the summer shutdown period of 2017. To avoid the transport of the superconducting wiggler, the replacement and vacuum welding of the chamber were carried out in the accelerator tunnel. The superconducting wiggler was restored to operation in October 2017.

Another trouble was the occurrence of corrosion on the copper water cooling pipe installed in the septum chamber as shown in **Fig. 5**. The injection septum magnet is placed at the left side of the beam chamber. The stored beam travels through the center of the chamber in front and the injection beam comes by penetrating the SUS foil. A copper plate with water cooling pipe is equipped at the left side wall which is irradiated by synchrotron radiation (SR). The leakage had been suppressed using a liquid seal for a while. However, the water cooling by adding an SR absorber at the upstream was stopped and the inside of the cooling pipe was evacuated. To solve the trouble completely, an upgrade with renewal of the septum magnet is in progress.

In the PF-AR, similar statistics are listed in **Table 5** and **Table 6**, and a pie chart of the down time in FY2017 is shown in **Fig. 6**. The MTBF was about 39 hours, and the failure rate was 1.2%. In FY2017, the number of failures significantly increased as shown in **Table 5**. About half of the failures were due to a sudden beam loss caused by dust trapping, and a beam dump (or loss) caused by accidental discharge of the injection kicker magnet accounted for 15 times. Dust trapping in the PF-AR has been observed especially just after a large reconstruction. Its frequency is expected to gradually decrease as the vacuum scrubbing proceeds. The accidental discharge of the kicker magnet without any injection trigger was an initial failure of the new injection kicker system. It could be eliminated by switching off the power supply. However, since it is incompatible with the top-up injection, the causes and countermeasures for noise are being investigated. As these frequently-occurring failures could be quickly recovered by re-injection, the mean downtime was as short as 0.4 h.

Full energy injection has become possible by completing the new direct beam transport line, and acceleration and deceleration between 3 GeV and 6.5 GeV are no longer needed. In addition, the injection has been carried out without interruption of user operation since December 2017.

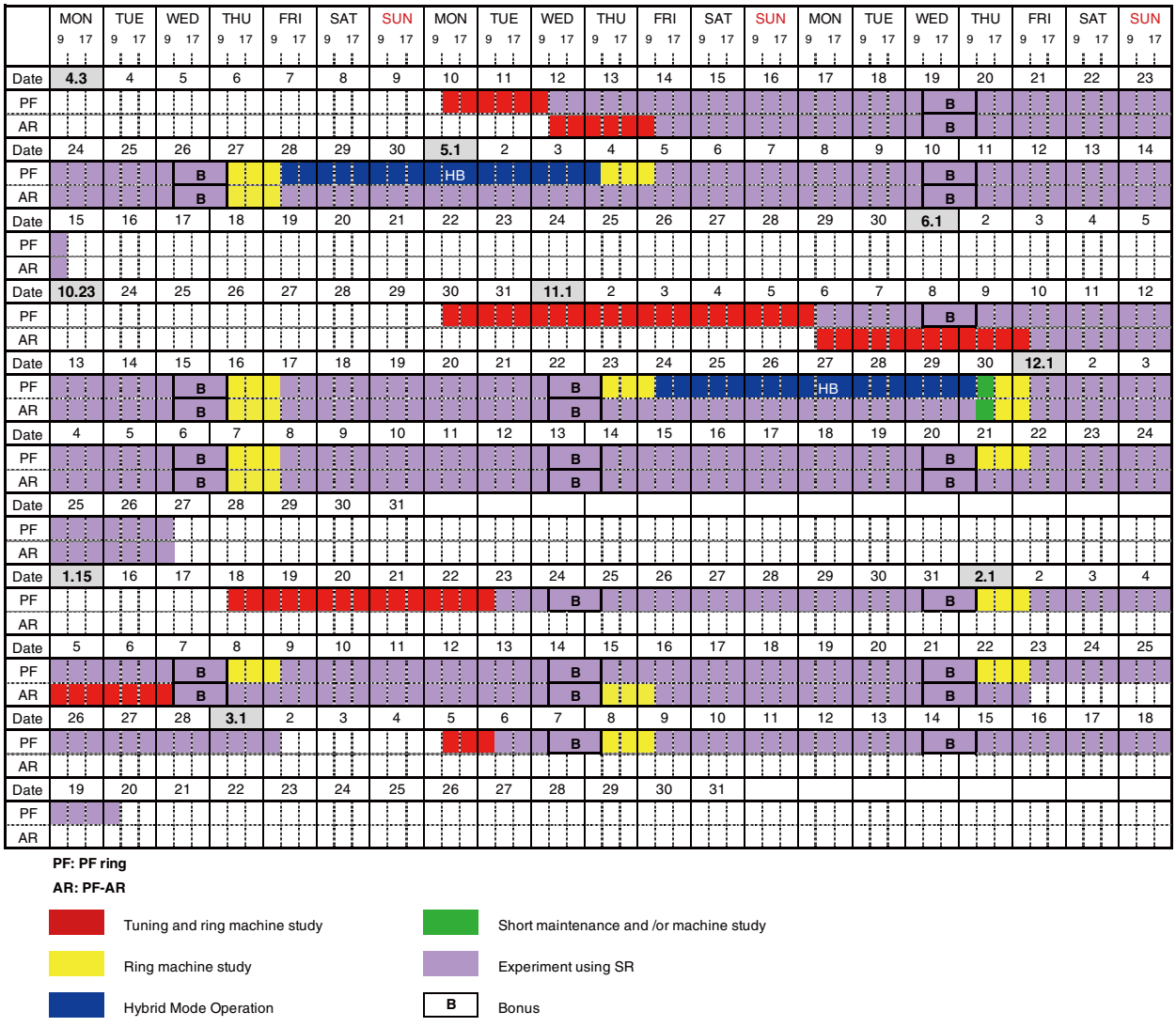

Figure 2: Operation schedule of PF ring and PF-AR in FY2017.

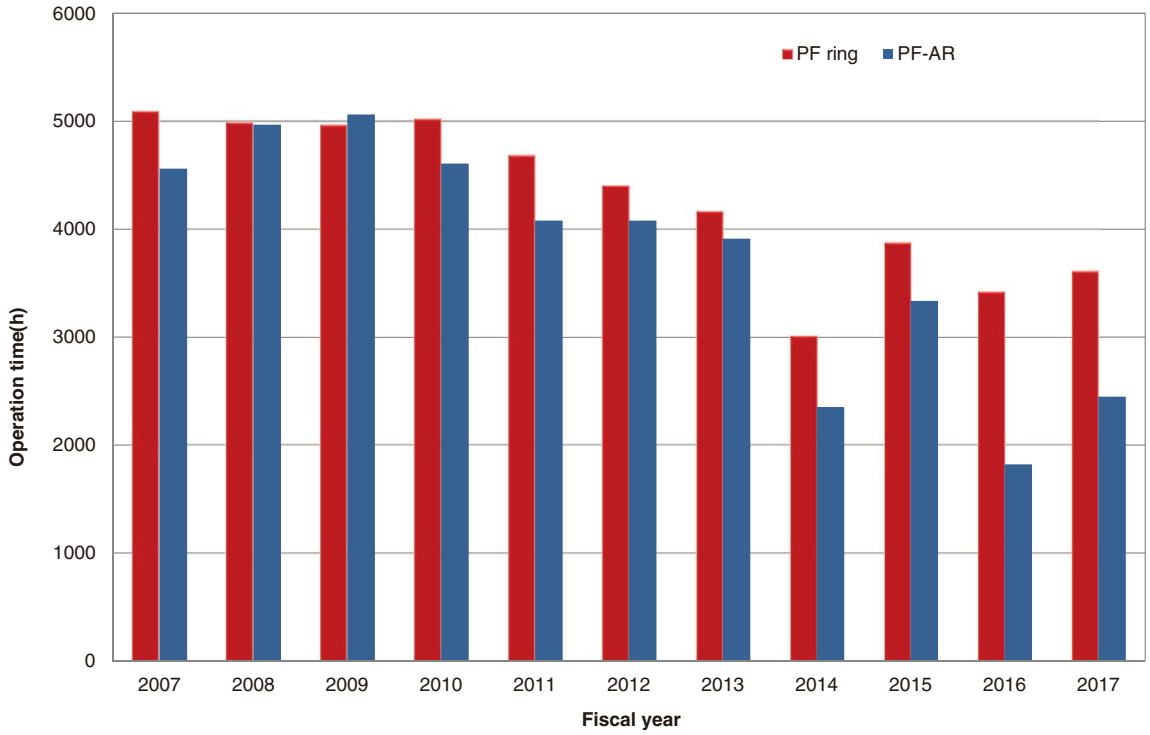

Figure 3: Total operation time for PF ring and PF-AR.

Table 3: Operation statistics for PF ring from FY2007 to FY2017.

Fiscal Year	2007	2008	2009	2010	2011	2012	2013	2014	2015	2016	2017
Total operation time (h)	5104	5000	4976	5064	4728	4416	4176	3024	3888	3432	3624
Scheduled user time (h)	4296	4032	4008	4080	2832	3792	3504	2328	3048	2928	3000
Ratio of user time (%)	84.2	80.6	80.5	80.6	59.9	85.9	83.9	77.0	78.4	85.3	82.8
No. of failures	23	18	24	18	18	23	22	15	23	18	14
Total down time (h)	91.1	23.8	42.7	29.2	14.9	37.6	52.1	11.4	14.4	17.3	16.6
Failure rate (%)	2.1	0.6	1.1	0.7	0.5	1.0	1.5	0.5	0.5	0.6	0.6
MTBF (h)	186.8	224.0	167.0	226.7	157.3	164.9	159.3	155.2	132.5	162.7	214.3
MDT (h)	4.0	1.3	1.8	1.6	0.8	1.6	2.4	0.8	0.6	1.0	1.2

Table 4: Number of failures for PF ring from FY2007 to FY2017.

Fiscal Year	2007	2008	2009	2010	2011	2012	2013	2014	2015	2016	2017
RF	4	5	12	13	5	10	8	1	1	1	1
Magnet	2	3	4	0	2	0	2	4	7	7	6
Injection	3	4	0	1	0	0	1	3	6	0	3
Vacuum	1	0	0	0	0	0	0	0	1	2	0
Dust trap	1	0	1	0	0	0	0	0	0	0	0
Insertion Devices	4	3	1	1	4	3	0	1	1	0	2
Control/ Monitor	0	0	3	0	1	6	5	3	3	5	0
Cooling water	0	1	1	0	0	0	0	0	0	0	0
Safety/ Beamline	2	1	2	2	1	1	1	3	2	1	1
Earthquake	2	1	0	0	4	3	1	0	2	2	0
Electricity	4	0	0	1	1	0	4	0	0	0	1
Total	23	18	24	18	18	23	22	15	23	18	14

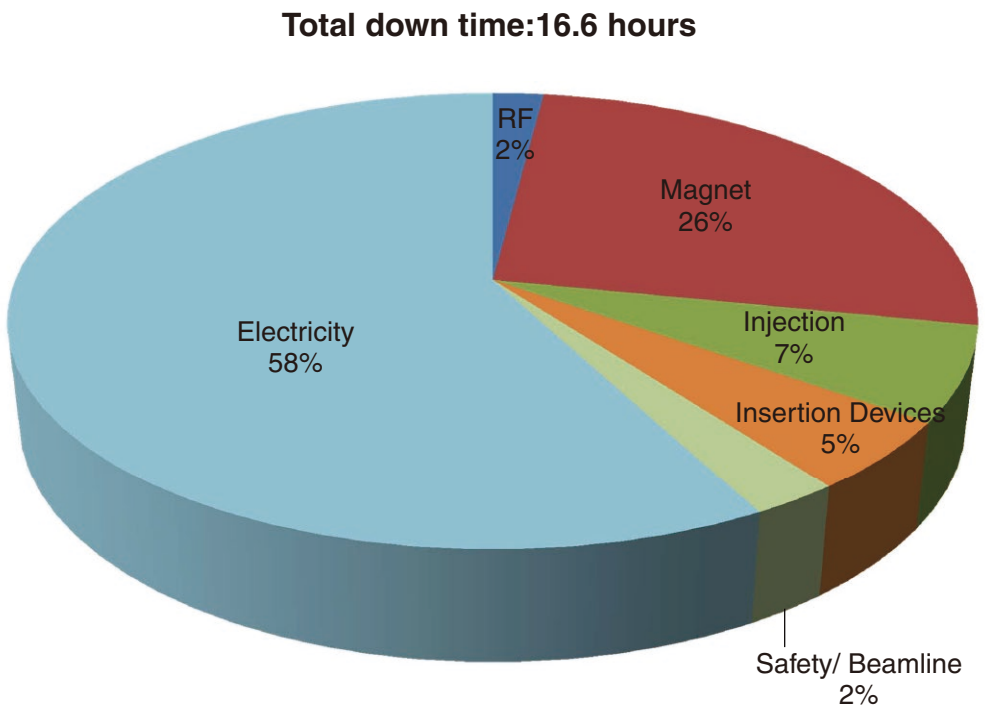

Figure 4: Pie chart of down time for PF ring in FY2017.

Table 5: Operation statistics for PF-AR from FY2007 to FY2017.

Fiscal Year	2007	2008	2009	2010	2011	2012	2013	2014	2015	2016	2017
Total operation time (h)	4561	4969	5063	4608	4080	4080	3912	2352	3336	1821	2448
Scheduled user time (h)	3624	4344	4392	4032	2904	3672	3478	1992	2784	1104	2136
Ratio of user time (%)	79.5	87.4	86.7	87.5	71.2	90.0	88.9	84.7	83.5	60.6	87.3
No. of failures	60	40	41	74	49	33	47	22	18	13	55
Total down time (h)	45.2	41.7	91.0	73.7	38.7	29.7	99.6	37.0	31.0	18.3	24.7
Failure rate (%)	1.2	1.0	2.1	1.8	1.3	0.8	2.9	1.9	1.1	1.7	1.2
MTBF (h)	60.4	108.6	107.1	54.5	59.3	111.3	74.0	90.5	154.7	84.9	38.8
Mean down time (h)	0.8	1.0	2.2	1.0	0.8	0.9	2.1	1.7	1.7	1.4	0.4

Table 6: Number of failures for PF-AR from FY2007 to FY2017.

Fiscal Year	2007	2008	2009	2010	2011	2012	2013	2014	2015	2016	2017
RF	1	4	8	10	5	4	5	2	1	3	5
Magnet	1	2	2	10	8	3	4	9	4	5	1
Injection	8	9	1	6	4	3	18	7	1	2	19
Vacuum	2	0	2	1	0	1	0	0	1	1	0
Dust trap	39	15	16	24	20	13	3	2	1	1	22
Insertion Devices	0	0	0	0	0	0	0	0	0	0	0
Control/ Monitor	1	1	1	2	1	2	8	0	0	0	0
Cooling water	0	3	4	4	1	0	2	0	0	0	0
Safety/ Beamline	5	5	7	17	3	4	3	1	8	0	8
Earthquake	1	0	0	0	5	3	1	0	2	1	0
Electricity	2	1	0	0	2	0	3	1	0	0	0
Total	60	40	41	74	49	33	47	22	18	13	55

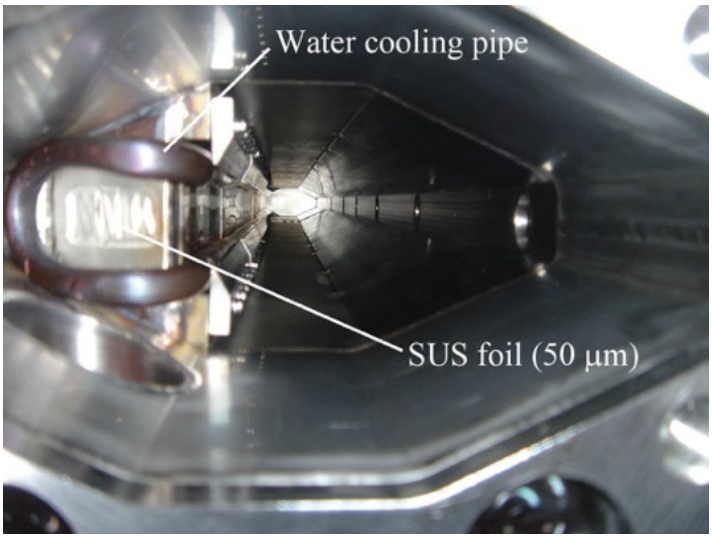

Figure 5: Photograph of the inside of the septum chamber.

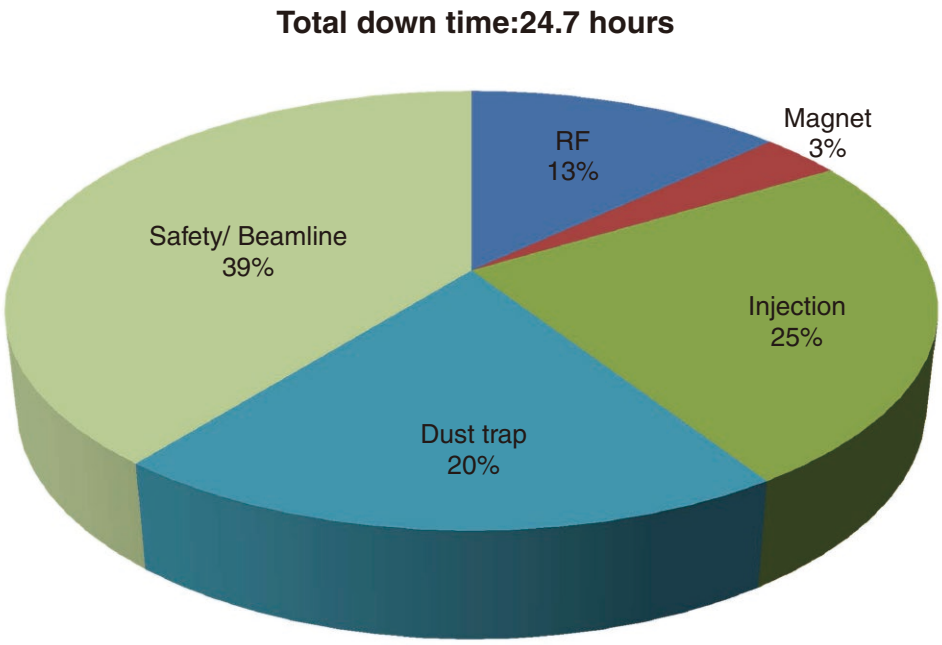

Figure 6: Pie chart of down time for PF-AR in FY2017.

3. Experimental Stations

Fifty-three experimental stations are in operation at the PF ring, PF-AR and slow positron facility (SPF), as shown in **Figs. 7**, **8** and **9**. Thirty-five stations are dedicated to research using hard X-rays, 14 stations for studies in the VUV and soft X-ray energy regions, and 4 stations for studies using slow positrons. **Tables 7**, **8** and **9** summarize the areas of research being carried out at the experimental stations at the PF ring, PF-AR and SPF.

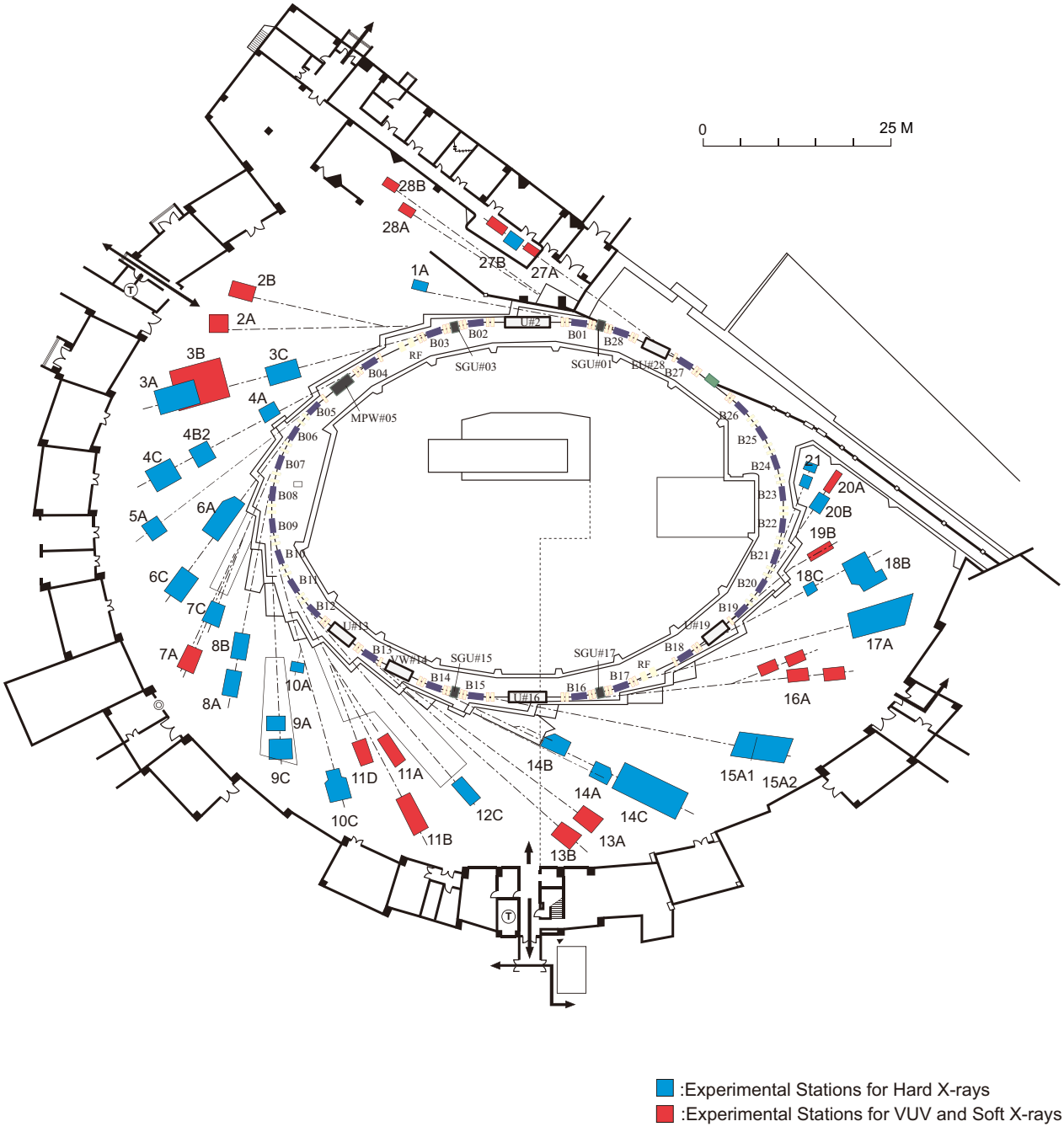

Figure 7: Plan view of the PF experimental hall, showing hard X-ray experimental stations (blue), and VUV and soft X-ray experimental stations (red).

Table 7: List of the experimental stations available for users at the PF ring.

Experimental Station		Person in Charge
BL-1	(Short Gap Undulator)	
A	Macromolecular crystallography	N. Matsugaki
BL-2	(Variable Polarization Undulator for VUV and planer undulator for SX)	
A	High-resolution VUV-SX beamline for angle-resolved photoemission spectroscopy	H. Kumigashira
B	High-resolution VUV-SX spectroscopies	H. Kumigashira
BL-3	(A: Short Gap Undulator)	
A	X-ray diffraction for material structural science	H. Nakao
B	VUV and soft X-ray spectroscopy (♠)	K. Edamoto [Rikkyo Univ.], J. Yoshinobu [The Univ. of Tokyo], K. Mase
C	Characterization of X-ray optical elements/White X-ray magnetic diffraction	K. Hirano
BL-4		
A	Trace element analysis, X-ray microprobe (♠)	Y. Takahashi [The Univ. of Tokyo], M. Kimura, Y. Niwa
B2	High resolution powder diffraction (♠)	H. Uekusa [Tokyo Inst. of Tech.], H. Nakao
C	X-ray diffraction for material structural science	H. Nakao
BL-5	(Multipole Wiggler)	
A	Macromolecular crystallography	N. Matsugaki
BL-6		
A	Small-angle X-ray scattering	N. Igarashi
C	X-ray diffraction and spectroscopy (♠)	M. Okube [Tohoku Univ.], H. Kawata
BL-7		
A	Soft X-ray spectroscopy (♦)	J. Okabayashi [RCS, The Univ. of Tokyo], K. Amemiya
C	X-ray spectroscopy and diffraction	H. Sugiyama
BL-8		
A	Weissenberg camera for powder/Single-crystal measurements under extreme conditions	H. Sagayama
B	Weissenberg camera for powder/Single-crystal measurements under extreme conditions	H. Sagayama
BL-9		
A	XAFS	H. Abe
C	XAFS	H. Abe
BL-10		
A	X-ray diffraction and scattering (♠)	A. Yoshiasa [Kumamoto Univ.], R. Kumai
C	Small-angle X-ray Scattering	N. Shimizu
BL-11		
A	Soft X-ray spectroscopy	Y. Kitajima
B	Soft X-ray spectroscopy	Y. Kitajima
D	Characterization of optical elements used in the VSX region♠	K. Mase
BL-12		
C	XAFS	H. Nitani

Experimental Station		Person in Charge
BL-13	(Variable Polarization Undulator)	
A/B	VUV and soft X-ray spectroscopies with circular and linear polarization	K. Mase
BL-14	(Vertical Wiggler)	
A	Crystal structure analysis and detector development	S. Kishimoto
B	High-precision X-ray optics	K. Hirano
C	Medical applications and general purpose (X-ray)	K. Hyodo
BL-15	(Short Gap Undulator)	
A1	Semi-microbeam XAFS	Y. Takeichi
A2	High brilliance small-angle X-ray scattering	N. Shimizu
BL-16	(Variable Polarization Undulator)	
A	Soft X-ray spectroscopies with circular and linear polarization	K. Amemiya
BL-17	(Short Gap Undulator)	
A	Macromolecular crystallography	Y. Yamada
BL-18		
B	Multipurpose monochromatic hard X-ray station (♦)	A. Bhattacharyya [SINP], R. Kumai
C	High pressure X-ray powder diffraction (DAC) (♠)	H. Kagi [The Univ. of Tokyo], N. Funamori
BL-19		
B	Test beamline	H. Nakao
BL-20		
A	VUV spectroscopy (◊)	N. Kouchi [Tokyo Inst. of Tech], J. Adachi
B	White & monochromatic X-ray topography and X-ray diffraction experiment	H. Sugiyama
BL-27	(Beamline for radioactive samples)	
A	Radiation biology, soft X-ray photoelectron spectroscopy	N. Usami
B	Radiation biology, XAFS	N. Usami
BL-28	(Variable Polarization Undulator)	
A	High-resolution angle-resolved photoemission spectroscopy with circular and linear polarization	K. Horiba
B	High-resolution VUV spectroscopies with circular and linear polarization	K. Horiba

♠ User group operated beamline
♦ External beamline
◊ Operated by University

RCS: Research Center for Spectrochemistry, the University of Tokyo
SINP: Saha Institute of Nuclear Physics

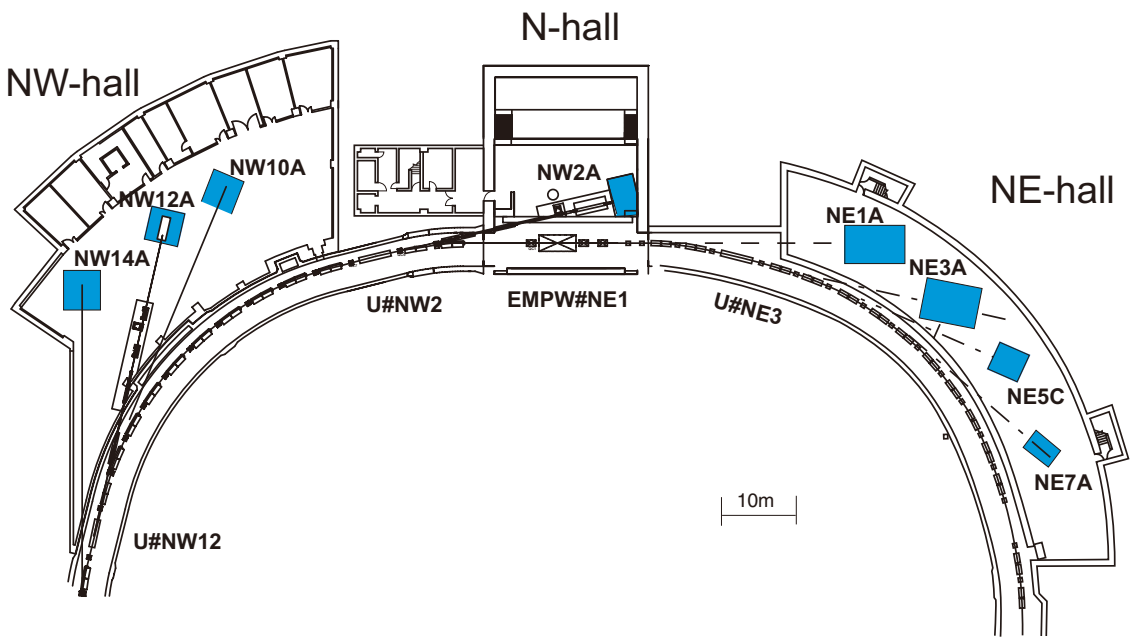

Figure 8: Plan view of the beamlines in the PF-AR north-east, north, and north-west experimental halls.

Table 8: List of the experimental stations at the PF-AR.

Experimental Station		Person in Charge
AR-NE1 A	(Multipole Wiggler) Laser-heating high pressure X-ray diffraction and nuclear resonant scattering (DAC)	N. Funamori
AR-NE3 A	(In-vacuum Undulator) Macromolecular crystallography	Y. Yamada
AR-NE5 C	High pressure and high temperature X-ray diffraction (MAX-80)	N. Funamori
AR-NE7 A	High pressure and high temperature X-ray diffraction (MAX-III) (♥), X-ray imaging	K. Hyodo, A. Suzuki [Tohoku Univ.]
AR-NW2 A	(In-vacuum Type Tapered Undulator) Time-resolved Dispersive XAFS/XAFS/X-ray Diffraction	Y. Niwa
AR-NW10 A	XAFS	H. Nitani
AR-NW12 A	(In-vacuum Type Tapered Undulator) Macromolecular crystallography	M. Hikita
AR-NW14 A	(In-vacuum Undulator) Time-resolved X-ray diffraction, scattering and absorption	S. Nozawa

♥ User group operated experimental equipment

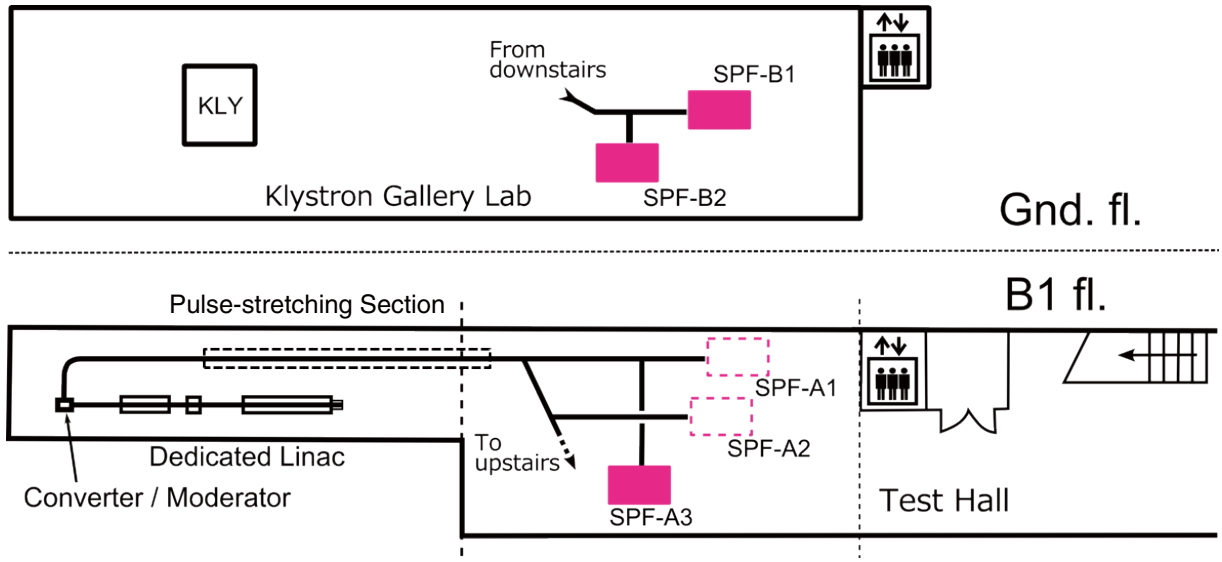

Figure 9: View of the beamlines in the Slow Positron Facility.

Table 9: List of the experimental stations in the Slow Positron Facility.

Experimental Station		Person in Charge
SPF-A3	Total-reflection high-energy positron diffraction	I. Mochizuki
SPF-A4	Low-energy positron diffraction	I. Mochizuki
SPF-B1	General purpose (Positronium laser cooling)	I. Mochizuki
SPF-B2	Positronium time-of-flight	I. Mochizuki

4. Summary of User Proposals

The Photon Factory accepts experimental proposals submitted by researchers mainly at universities and research institutes inside and outside Japan. The PF Program Advisory Committee (PF-PAC) reviews the proposals, and the Advisory Committee for the Institute of Materials Structure Science approves those that are favorably recommended. The number of accepted proposals over the period 2006–2017 is shown in **Table 10**, where S1/S2, U, G, P, and MP denote Special, Urgent, General, Preliminary, and Multi-Probe proposals, respectively. Category T is a new type of proposal for supporting researches by PhD students. Category MP is also a new type of proposal in which no less than two of the four beams, synchrotron radiation at the PF, slow positron beam at the Slow Positron Facility, and neutron and muon beams at the Materials and Life Science Experimental Facility (MLF) in J-PARC, are required to be used, as a multi-probe experiment.

Category C is a proposal for collaboration between KEK and a research institute including a private company. Category I is a non-proprietary proposal for the integrated promotion of social system reform and research and development, supported by the Ministry of Education, Culture, Sports, Science and Technology (from 2009 to 2015). Category V is a non-proprietary grant-aided proposal that has already been reviewed and approved for a research grant; beam time for proposals in this category is allocated with high priority, and applicants are required to pay the regulation fees for the beam time. Category Y is a proprietary proposal; applicants are required to pay the regulation fees for the beam time. The number of current G-type proposals each year has exceeded 760 for the past few years. In addition to these proposals, 15 projects in the Platform for Drug Discovery, Informatics, and Structural Life Science were performed at the PF in FY2017. A full list of the proposals effective in FY2017 and their scientific output can be found in the Photon Factory Activity Report (https://www2.kek.jp/imss/pf/science/publ/acrpubl.html).

Table 10: Number of proposals accepted for the period 2006–2017.

category	FY-2006	2007	2008	2009	2010	2011	2012	2013	2014	2015	2016	2017
S1	1	0	0	0	0	0	0	0	0	0	0	0
S2	6	1	4	6	3	2	4	5	4	7	6	1
U	1	7	3	2	2	0	4	1	0	1	0	1
G	386	403	402	397	407	415	454	447	407	361	372	392
P	22	14	14	14	16	11	18	18	5	16	10	16
T									6	4	3	3
MP										4	0	0
C	25	24	18	12	15	19	20	20	25	24	19	21
I				9	17	13	17	13	16	11	-	-
V							1	2	2	2	4	4
Y	23	23	22	29	31	30	30	41	22	33	39	30

S-type proposals consist of two categories, S1 and S2. S1 proposals are self-contained projects of excellent scientific quality, and include projects such as the construction and improvement of beamlines and experimental stations which will be available for general users after the completion of the project. S2 proposals are superior-grade projects that require the full use of synchrotron radiation or long-term beam time. Proposals are categorized into five scientific disciplines, and reviewed by the five subcommittees of PF-PAC: 1) electronic structure, 2) structural science, 3) chemistry and materials, 4) life science I (protein crystallography), and 5) life science II (including soft matter science). **Figure 10** shows the distribution by research field of the proposals accepted by the subcommittees in FY2017.

The number of users for all types of proposals exceeds 3,000. About 20% of the proposals are conducted by new spokespersons, which indicates that the Photon Factory is open to public academic users. **Figure 11** shows the distribution of users by institution and their positions. Over three-quarters of the users belong to universities. Over two-thirds of the national university users are graduate and undergraduate students; this clearly shows that the Photon Factory plays an important role in both research and education. The geographical distribution of the Photon Factory users is shown in **Figs. 12** and **13**, which also indicates the immense contribution of the Photon Factory to research and education throughout Japan. The registered number of papers published in 2017 based on experiments at the PF was 533 at the time of writing (July 1st, 2018). In addition, 57 doctoral and 214 master theses have been presented.

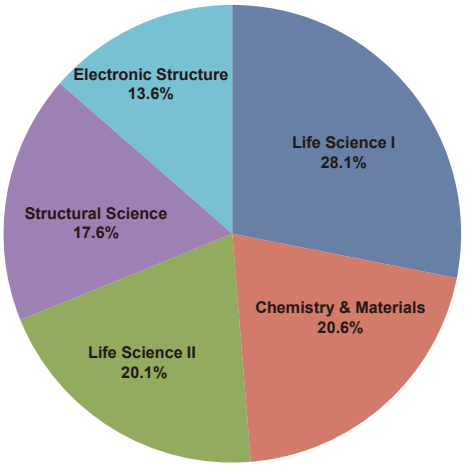

Figure 10: Distribution by scientific field of experimental proposals accepted in FY2017.

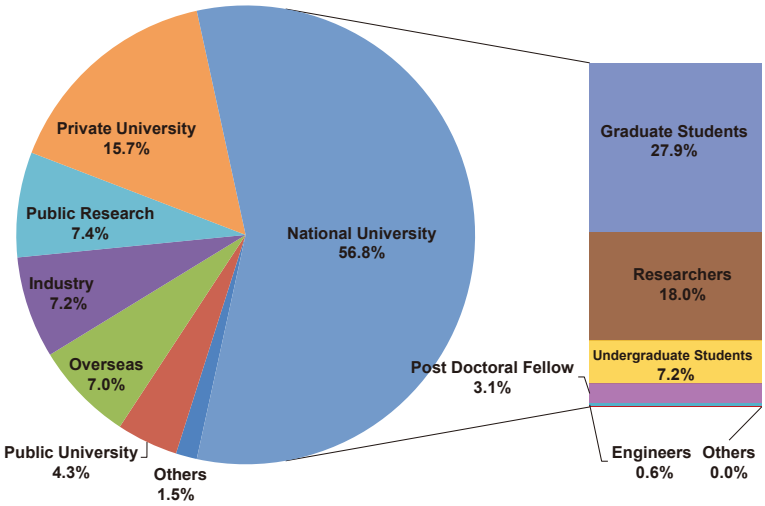

Figure 11: Distribution of users by institution and position.

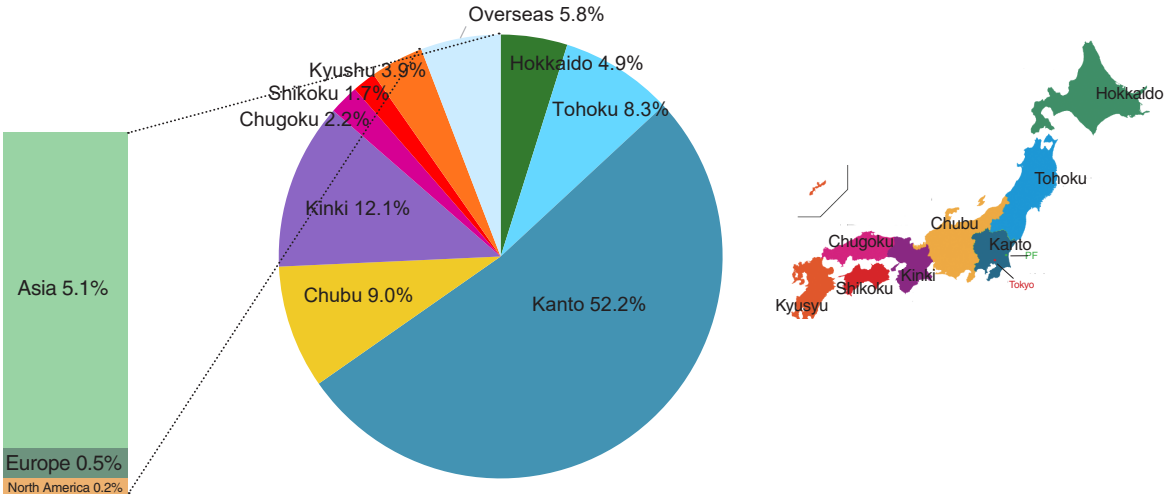

Figure 12: Regional distribution of spokespersons of proposals accepted in FY2017. We corrected the pie chart on 2019/09/02.

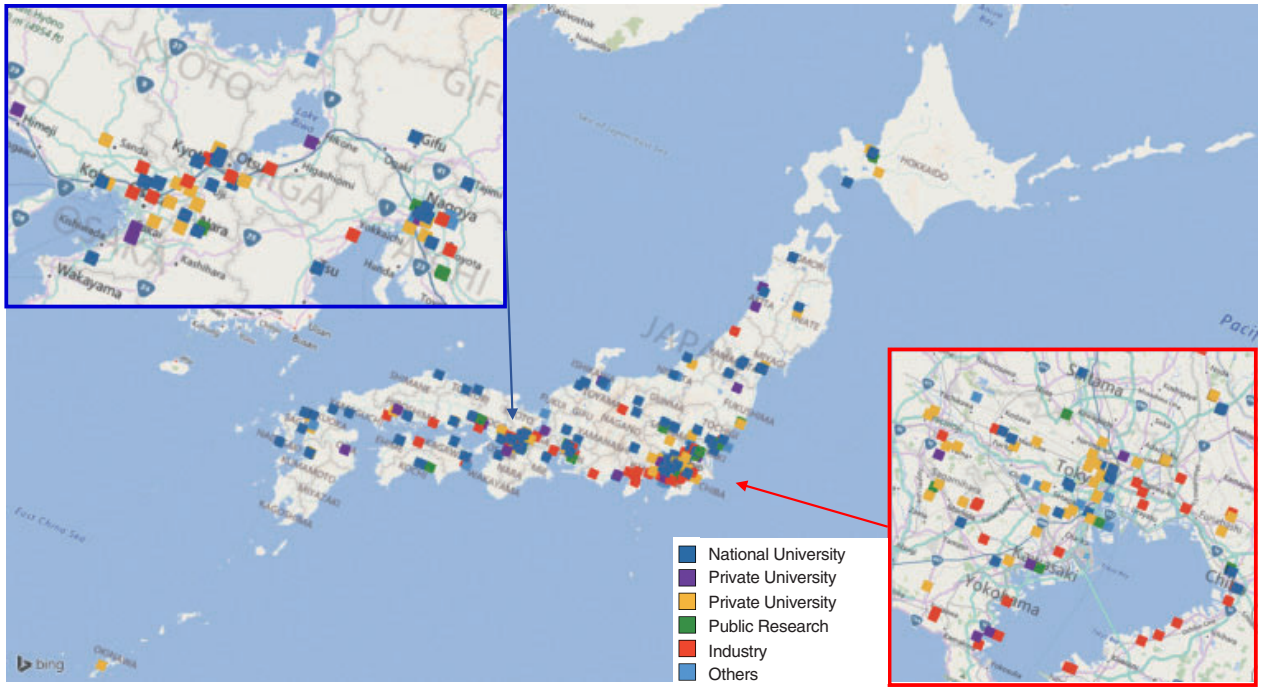

Figure 13: Geographical distribution of Photon Factory users in FY2017 (domestic users only).